Inorg. Chem. **2003**, *42*, 1076–1086

Reduction Pathway of End-On Coordinated Dinitrogen. 3.† Electronic Structure and Spectroscopic Properties of Molybdenum/Tungsten Hydrazidium Complexes‡

Kay H. Horn, Nicolai Lehnert, and Felix Tuczek*

Institut für Anorganische Chemie, Christian Albrechts Universität, D-24098 Kiel, Germany

Received July 15, 2002

The spectroscopic properties and electronic structure of the hydrazidium complexes $[MF(NNH_3)(depe)_2](BF_4)_2$, M = Mo and W, are investigated (depe = 1,2-bis(diethylphosphino)ethane). Vibrational spectroscopic data for both compounds are evaluated with a quantum-chemistry-assisted normal coordinate analysis, giving an N–N force constant of 6.03 mdyn/Å and metal–N force constants of 8.01 (Mo–N) and 7.31 mdyn/Å (W–N), respectively. On the basis of these results and DFT calculations on a $[MoF(NNH_3)(PH_3)_4]^{2+}$ model system, the N–N bond order in these systems is 1 (single σ bond) and metal–N bonding corresponds to a triple bond. The metal centers are assigned a +IV oxidation state (d^2 configuration) and the NNH_3 ligand is assigned a –1 formal charge which by σ- and π-donation to the metal is reduced to +0.48. The two metal-d electrons are located in the nonbonding (n) d_{xy} orbital. This bonding description is supported by the results of optical absorption spectroscopy showing the n $\rightarrow$ (metal–ligand)π^* transition at 536 nm (not observed in the tungsten compound) and the (metal–ligand)$\pi \rightarrow$ (metal–ligand)π^* transition at 251 nm for the $MoNNH_3$ and at 237 nm for the $WNNH_3$ complex. The activation enthalpy for splitting of the N–N bond in these systems to generate NH_4^+ is estimated to be larger than 40 kcal/mol. Hydrazidium complexes with diphosphine coligands are therefore inert with respect to N–N cleavage and thus represent the ultimate stage of N_2 reduction at six-coordinate d^6 metal centers in the absence of external reductants.

Introduction

In preceding publications dealing with the reduction and protonation of dinitrogen at transition-metal centers, we have used spectroscopy and DFT calculations to obtain insight into elemental reaction steps involved in this chemistry.[1] In particular, we have made a distinction between "symmetric" and "asymmetric" pathways. The symmetric pathway starts from N_2 coordinated in μ-1,2 (linear bridging), η^2 (side-on coordinated), or μ-η^2:η^2 (side-on/edge-on bridging) fashion and primarily leads to coordinated diazene and hydrazine.[2] In the framework of this reaction mode, we have spectroscopically characterized Fe(II) trans μ-1,2-diazene dimers with thiolate/thioether coligands.[3] The symmetric pathway also comprises systems in the extreme activation limit which spontaneously cleave the N_2 molecule coordinated in an end-on (μ-1,2) or side-on (μ-η^2:η^2) bridging manner into two nitrido species.[4] The asymmetric pathway is based on dinitrogen coordinated end-on terminally to transition metals and after six protonation steps leads to ammonia. If "moderately" activating complexes containing Mo and W phosphine systems are employed, all the intermediates along the reduction pathway can be isolated (see Scheme 1).[5]

* To whom correspondence should be addressed. E-mail: ftuczek@ac.uni-kiel.de.

† For parts 1 and 2, see ref 1.

‡ Dedicated to Prof. Dr. R. Mews on the occasion of his 60th birthday.

(1) (a) Lehnert, N.; Tuczek, F. *Inorg. Chem.* **1999**, *38* (9), 1659. (b) Lehnert, N.; Tuczek, F. *Inorg. Chem.* **1999**, *38* (9), 1671. (c) Tuczek, F.; Lehnert, N. *Angew. Chem., Int. Ed.* **1998**, *37*, 2636−2638.

(2) (a) Fryzuk, M.; Johnson, S. A. *Coord. Chem. Rev.* **2000**, *200*, 379−419. (b) Sellmann, D.; Utz, J.; Blum, N.; Heinemann, F. W. *Coord. Chem. Rev.* **1999**, *190−192* (0), 607. (c) Hidai, M.; Mizobe, Y. *Chem. Rev.* **1995**, *95*, 1115.

(3) Lehnert, N.; Wiesler, B. E.; Tuczek, F.; Hennige, D.; Sellmann, D. *J. Am. Chem. Soc.* **1997**, *119*, 8879.

(4) (a) Laplaza, C. E.; Cummins, C. C. *Science* **1995**, *268*, 861. (b) Laplaza, C. E.; Johnson, M. J. A.; Peters, J. C.; Odom, A. L.; Kim, E.; Cummins, C. C. *J. Am. Chem. Soc.* **1996**, *118*, 8623. (c) Laplaza, C. E.; Johnson, A. R.; Cummins, C. C. *J. Am. Chem. Soc.* **1996**, *118*, 709. (d) Caselli, A.; Solari, E.; Scopelliti, R.; Floriani, C.; Re, N.; Rizzoli, C.; Chiesi-Villa, A. *J. Am. Chem. Soc.* **2000**, *122*, 3652. (e) Clentsmith, G. K. B.; Bates, V. M. E.; Hitchcock, P. B.; Cloke, F. G. N. *J. Am. Chem. Soc.* **1999**, *121*, 10444.

(5) (a) Leigh, G. J. *Acc. Chem. Res.* **1992**, *25*, 177. (b) Henderson, R. A.; Leigh, G. J.; Pickett, C. *Adv. Inorg. Chem. Radiochem.* **1983**, *27*, 197−292.

10.1021/ic020458x CCC: $25.00
Published on Web 01/22/2003

Scheme 1. Reduction Pathway of End-On Terminally Coordinated Dinitrogen

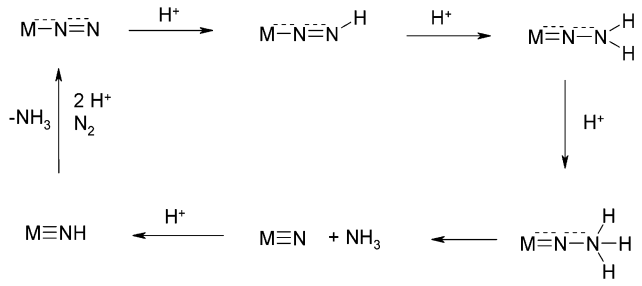

This reaction sequence has been suggested to apply to nitrogenase as it is compatible with the Thorneley/Lowe kinetic scheme.[6] Previously, we have studied the N_2, N_2H, and N_2H_2 complexes $[M(N_2)_2(dppe)_2]$, $[MF(NNH)(dppe)_2]$, and $[MF(NNH_2)(dppe)_2]^+$ (M = Mo, W; dppe = 1,2-bis(diphenylphosphino)ethane) with the help of infrared and Raman spectroscopy coupled to DFT calculations and found that this reaction pathway is characterized by a stepwise flow of charge from the metal to the N_2/N_2H_x ligand and a concomitant increase of metal−ligand covalency.[1a,b] The major part of metal-to-ligand charge transfer occurs after the first protonation step leading to coordinated diazenide(−). Addition of the second proton is only accompanied by a minor change of covalency, generating an almost neutral NNH_2 species which is better described as coordinated isodiazene compared to the usual hydrazido(2−) formulation. These electronic structure descriptions are supported by the results of vibrational spectroscopy. The N−N and metal−N force constants evolve from 16.4 and 2.65 mdyn/Å in the N_2 complex to 7.20 and 6.31 mdyn/Å in the NNH_2 compound, respectively, indicating that the decrease in N−N bond order from 3 (N_2 complex) to 2 (NNH_2 complex) goes along with a more than doubled metal−N bond strength. As the NNH_2 ligand is almost neutral, the metal carries a formal charge of +2 in the corresponding complex, i.e., has donated two electrons to the N_2 ligand. These electrons are used to convert the π and π^* orbitals within the NNH_2 plane into a (filled) NH bonding orbital on N^{β} (terminal N) and a doubly occupied p donor orbital (lone pair) on N^{α} (coordinating N). In contrast, the N_2 out-of plane (vertical) orbitals π_v (filled) and π^*_v (empty) still exist at this stage, π^*_v being involved in back-bonding interaction between the metal and the N_2H_2 ligand.

Addition of one more proton to the NNH_2 complex generates the hydrazidium species which is the last intermediate before cleavage of the N−N bond (cf. Scheme 1). It is known that these intermediates form upon protonation of tungsten N_2 complexes containing strongly electron-donating phosphine ligands, employing strong acids in a large excess. Well-defined hydrazidium compounds described in the literature are $[WF(NNH_3)(depe)_2](BF_4)_2$ (**VI**), which has been characterized by NMR, elemental analysis and conductometry,[7] and $[WCl(NNH_3)(PMe_3)_4]Cl_2$ (**VII**), which has provided the first structural characterization of an NNH_3 system.[8] As our earlier investigations on Mo/W−N_2H_x complexes were based on systems containing bidentate phosphine coligands (i.e., dppe = 1,2-bis(diphenylphosphino)ethane), we decided to focus on complex **VI**, which is generated by protonation of the dinitrogen complex $[W(N_2)_2(depe)_2]$ (**IV**) with HBF_4. Similar NNH_3 complexes with dppe do not exist since protonation of the corresponding N_2 precursors stops at the NNH_2 stage. We also prepared the molybdenum analogue of **VI**, $[MoF(NNH_3)(depe)_2](BF_4)_2$ (**III**), by protonation of $[Mo(N_2)_2(depe)_2]$ (**I**) with HBF_4. The characterization of the Mo and W hydrazidium complexes **III** and **VI** by vibrational and optical spectroscopy is the subject of this paper. The analogous NNH_2 complexes $[MoCl(NNH_2)(depe)_2]Cl$ (**II**) and $[WCl(NNH_2)(depe)_2]Cl$ (**V**) were prepared by protonation of **I** and **IV** with HCl and for comparison studied by optical spectroscopy as well.

All spectroscopic results are interpreted by DFT calculations, providing information relevant to the electronic structure and reactivity of Mo and W hydrazidium compounds. In particular, the vibrational data are evaluated by a quantum-chemistry-assisted normal coordinate analysis (QCA-NCA), which we have developed earlier to account for the vibational properties of Mo/W−N_2, −N_2H, and −N_2H_2 compounds.[1a] Application of this method to the NNH_3 complexes allows one to monitor the evolution of force constants after the NNH_2 stage. Using time-dependent DFT, the electronic-structure calculations further allow one to calculate electronic transitions which are compared to the optical absorption data of the NNH_3 complexes **III**/**VI** and the corresponding NNH_2 complexes **II**/**V**, respectively. The implications of the resulting bonding description are discussed with respect to the reactivity of NNH_3 systems and their role in the end-on terminal reduction pathway of N_2.

Experiental and Computational Procedures

Sample Preparation and Isotopic Substitution. The natural isotope abundance dinitrogen complexes $[Mo(N_2)_2(depe)_2]$ **(Ia)** and $[W(N_2)_2(depe)_2]$ **(IVa)** were prepared by following literature procedures.[9] For the synthesis of the corresponding NNH_2 species $[MoCl(NNH_2)(depe)_2]Cl$ **(IIa)** and $[WCl(NNH_2)(depe)_2]Cl$ **(Va)**, anhydrous HCl was condensed onto the dinitrogen complexes **Ia** and **IVa** at −196 °C similar to a procedure described by Galindo.[8] $[MoF(NNH_3)(depe)_2](BF_4)_2$ **(IIIa)** and $[WF(NNH_3)(depe)_2](BF_4)_2$ **(VIa)** were obtained by protonation of **Ia** and **IVa**, respectively, with HBF_4.[7] Identity of **III** and **VI** was checked by fluorine analysis. The ^{15}N isotopomers $[Mo(^{15}N_2)_2(depe)_2]$ **(Ib)** and $[W(^{15}N_2)_2(depe)_2]$ **(IVb)** were synthesized using $^{15}N_2$. The preparation of the protonated, ^{15}N-labeled complexes $[MoCl(^{15}N^{15}NH_2)(depe)_2]Cl$ **(IIb)**, $[WCl(^{15}N^{15}NH_2)(depe)_2]Cl$ **(Vb)**, $[MoF(^{15}N^{15}NH_3)(depe)_2](BF_4)_2$ **(IIIb)**, and $[WF(^{15}N^{15}NH_3)(depe)_2](BF_4)_2$ **(VIb)** was carried out from the ^{15}N-substituted dinitrogen complexes **Ib** and **IVb**, respectively. The reactions and sample preparations were performed under a nitrogen or argon atmosphere using Schlenk techniques.

(6) Thorneley, R. N. F.; Lowe, D. J. In *Molybdenum Enzymes*; Spiro, T. G., Ed.; John Wiley: New York, 1985.

(7) Barclay; Hills; Hughes; Leigh; Macdonald; Bakar; Ali. *J. Chem. Soc., Dalton Trans.* **1990**, 2503.

(8) (a) Galindo; Hills; Hughes; Richards. *J. Chem. Soc., Dalton Trans.* **1990**, 283. (b) Galindo, A.; Hills, A.; Hughes, D. L.; Richards, R. L. *J. Chem. Soc., Chem Commun.* **1987**, 1815.

(9) Hussain, W.; Leigh, G. J.; Mohd Ali, H.; Pickett, C. J.; Rankin, D. A. *J. Chem. Soc., Dalton Trans.* **1984**, 1703.

The sample manipulations for vibrational and optical spectroscopy were carried out in a glovebox. All solvents were dried under argon.

IR Spectroscopy. Middle-infrared **(**MIR) spectra were obtained on KBr pellets using a Mattson Genesis Type I spectrometer. Far-infrared (FIR) spectra were obtained on RbI pellets using a Bruker IFS 66s FTIR spectrometer. Both instruments are equipped with a cryogenic (CTI) helium cryostat. The spectra were recorded at 10 K, and the resolution was set to 2 cm^{-1}.

UV/Vis Spectroscopy. Optical absorption spectra were obtained on neat compounds pressed between sapphire windows or from KBr pellets. The spectra were recorded at 10 K using a Varian Cary 5 UV−vis−NIR spectrometer equipped with a CTI cryocooler.

Normal Coordinate Analysis. Normal coordinate calculations were performed using the QCPE computer program 576 by Peterson and McIntosh. It involves solution of the secular equation $GFL = \Lambda L$ by the diagonalization procedure of Miyazawa.[10] The calculations are based on a general valence force field, and the force constants are refined using the nonlinear optimization routine of the simplex algorithm according to Nelder and Mead.[11] Normal coordinate analysis is based on the QCA-NCA procedure which involves generation of an initial force field by DFT methods.[1a]

For the hydrazidium complexes $[MF(NNH_3)(depe)_2](BF_4)_2$ (M = Mo (**III**) and W (**VI**)), model $[MoF(NNH_3)(PH_3)_4]^{2+}$ **(ĨĨI)** was employed for DFT calculations, giving theoretical frequencies and the matrix of force constants, $\tilde{f}$ (see below). To remove interactions between the PH_3 groups and the rest of the molecule, the PH_3 ligands were simplified to P atoms, leading to model $[MoF(NNH_3)P_4]^{2+}$ **(III′)** which was used for NCA. The corresponding *f*-matrix *f* ′ can be divided into two parts: force constants of the F−M−N−NH_3 unit (core); force constants of the MP_4 unit (frame). The force constants of the frame and nondiagonal elements between the core and the frame were taken from the DFT calculation and fixed. Very small matrix elements were neglected. The force constants of the core were fitted to match the experimental frequencies of **III** and **VI**, respectively, taking the DFT values as an initial guess.

DFT Calculations. Spin-restricted DFT calculations were performed for the NNH_3^- ligand and the NNH_2 and NNH_3 model systems $[MoF(NNH_2)(PH_3)_4]^+$ (**ĨI**) and $[MoF(NNH_3)(PH_3)_4]^{2-}$ (**ĨĨI**), respectively, using Becke's three parameter hybrid functional with the correlation functional of Lee, Yang, and Parr (B3LYP).[12] The LANL2DZ basis set was used for the calculations. It applies Dunning/Huzinaga full double-ζ (D95)[13] basis functions on the first row and Los Alamos effective core potentials plus DZ functions on all other atoms.[14] Charges are analyzed using the natural bond orbital (NBO) formalism (natural population analysis, NPA).[15] Transition energies are determined using time dependent DFT (TDDFT) calculations. All computational procedures are used as they are implemented in the Gaussian98 package.[16] Wave functions are plotted with the visualization program Molden.[17] The *f* matrix in internal coordinates is extracted from the Gaussian output using the program Redong.[18] The structure of **ĨĨI** used for TDDFT and the calculation of vibrational frequencies is obtained from a geometry optimization. Structure **ĨI** is only used for TDDFT and not optimized.

Results and Analysis

1. Synthesis. When a solution of $[W(N_2)_2(depe)_2]$ (**IV**) in benzene is reacted with 10 equiv of HBF_4 (ethereal solution), a red-pink precipitate is formed which has been analyzed and characterized by NMR as $[WF(NNH_3)(depe)_2](BF_4)_2$ (**VI**).[7] The same reaction carried out with $[Mo(N_2)_2(depe)_2]$ (**I**) gives a pink precipitate which according to fluorine analysis and vibrational spectroscopy (see below) is the Mo analogue of **VI**, $[MoF(NNH_3)(depe)_2](BF4)_2$ (**III**). ^{15}N substitution of the natural isotope abundance compounds **IIIa** and **IVa** giving compounds **IIIb** and **IVb**, respectively, was performed on the basis of the respective ^{15}N-substituted Mo− and W−bis(dinitrogen) complexes **Ia** and **IVa**. Reaction of these complexes with HCl analogous to the procedure described by Galindo for the preparation of the hydrazidium complex $[WCl(NNH_3)(PMe_3)_4]Cl_2$ (**VII**)[8] was found to generate the NNH_2 complexes $[MoCl(NNH_2)(depe)_2]Cl$ (**II**) (color: pink) and $[WCl(NNH_2)(depe)_2]Cl$ (**IV**) (color: orange-pink), respectively.

2. Vibrational Structure. **Spectral Analysis.** Raman spectra of **III** and **VI** were found to be almost featureless. Vibrational analysis is therefore exclusively based on the infrared spectra of **III** and **VI**. This corresponds to the situation encountered for $[WF(NNH_2)(dppe)_2](BF_4)$ and $[WF(NNH)(dppe)_2]$.[1a] Overview IR spectra of **IIIa** and **VIa** are shown in Figure 1; sections of the spectra showing isotopic shifts are given in Figure 2. Frequencies and assignments are collected in Tables 1 for **III** and 2 for **VI**.

Spectral comparison between **IIIa** and **IIIb** (Figure 2) shows three bands of **IIIb** which are absent in **IIIa**. The shoulder at 1347 cm^{-1} is assigned to the N−N stretch ν(NN), which is of low intensity as in the $[WF(NNH_2)(dppe)]^+$ complex.[1a] The Mo−N stretch is assigned to the shoulder at 591 cm^{-1}, in accordance with the W complex showing the metal−N stretch at 570 cm^{-1} (see below). Another feature of low intensity appearing at 434 cm^{-1} in the far-IR spectrum of **IIIb** is assigned to the doubly degenerate bending vibration of the linear Mo−N−N unit ("linear bend", δ(MoNN)). In the region of N−H stretching vibrations bands are found at 3315, 3265, and 3171 cm^{-1}, which upon isotopic substitution

(10) Miyazawa, T. J. *Chem. Phys*. **1958**, *29*, 246.
(11) Nelder, J. A.; Mead, R. *Comput. J*. **1965**, *7*, 308.
(12) Becke, A. D. *J. Chem. Phys.* **1993**, *98*, 5648.
(13) Dunning, T. H., Jr.; Hay, P. J. In *Modern Theoretical Chemistry*; Schaefer, H. F., III, Ed.; Plenum: New York, 1976.
(14) (a) Hay, P. J.; Wadt, W. R. *J. Chem. Phys.* **1985**, *82*, 270, 299. (b) Wadt, W. R.; Hay, P. J. *J. Chem. Phys.* **1985**, *82*, 284.
(15) (a) Foster, J. P.; Weinhold, F. *J. Am. Chem. Soc*. **1980**, *102*, 7211. (b) Rives, A. B.; Weinhold F. *Int. J. Quantum Chem. Symp.* **1980**, *14*, 201. (c) Reed, A. E.; Weinstock, R. B.; Weinhold, F. *J. Chem. Phys.* **1985**, *83*, 735. (d) Reed, A. E.; Curtiss, L. A.; Weinhold, F. *Chem. Rev.* **1988**, *88*, 899.
(16) Frisch, M. J.; Trucks, G. W.; Schlegel, H. B.; Scuseria, G. E.; Robb, M. A.; Cheeseman, J. R.; Zakrzewski, V. G.; Montgomery, J. A., Jr.; Stratmann, R. E.; Burant, J. C.; Dapprich, S.; Millam, J. M.; Daniels, A. D.; Kudin, K. N.; Strain, M. C.; Farkas, O.; Tomasi, J.; Barone, V.; Cossi, M.; Cammi, R.; Mennucci, B.; Pomelli, C.; Adamo, C.; Clifford, S.; Ochterski, J.; Petersson, G. A.; Ayala, P. Y.; Cui, Q.; Morokuma, K.; Malick, D. K.; Rabuck, A. D.; Raghavachari. K.; Foresman, J. B.; Cioslowski, J.; Ortiz, J. V.; Baboul, A. G.; Stefanov, B. B.; Liu, G.; Liashenko, A.; Piskorz, P.; Komaromi, I.; Gomperts, R.; Martin, R. L.; Fox, D. J.; Keith, T.; Al-Laham, M. A.; Peng, C. Y.; Nanayakkara, A.; Gonzalez, C.; Challacombe, M.; Gill, P. M. W.; Johnson, B.; Chen, W.; Wong, M. W.; Andres, J. L.; Gonzalez, C.; Head-Gordon, M.; Replogle, E. S.; Pople, J. A. *Gaussian 98*, revision A.7; Gaussian, Inc.: Pittsburgh, PA, 1998.
(17) Schaftenaar, G. *Molden*, version 3.2; CAOS/CAMM Center, University of Nijmegen: Nijmegen, The Nederlands.
(18) Allouche, A.; Pourcin, J. *Spectrochim. Acta* **1993**, *49A*, 571.

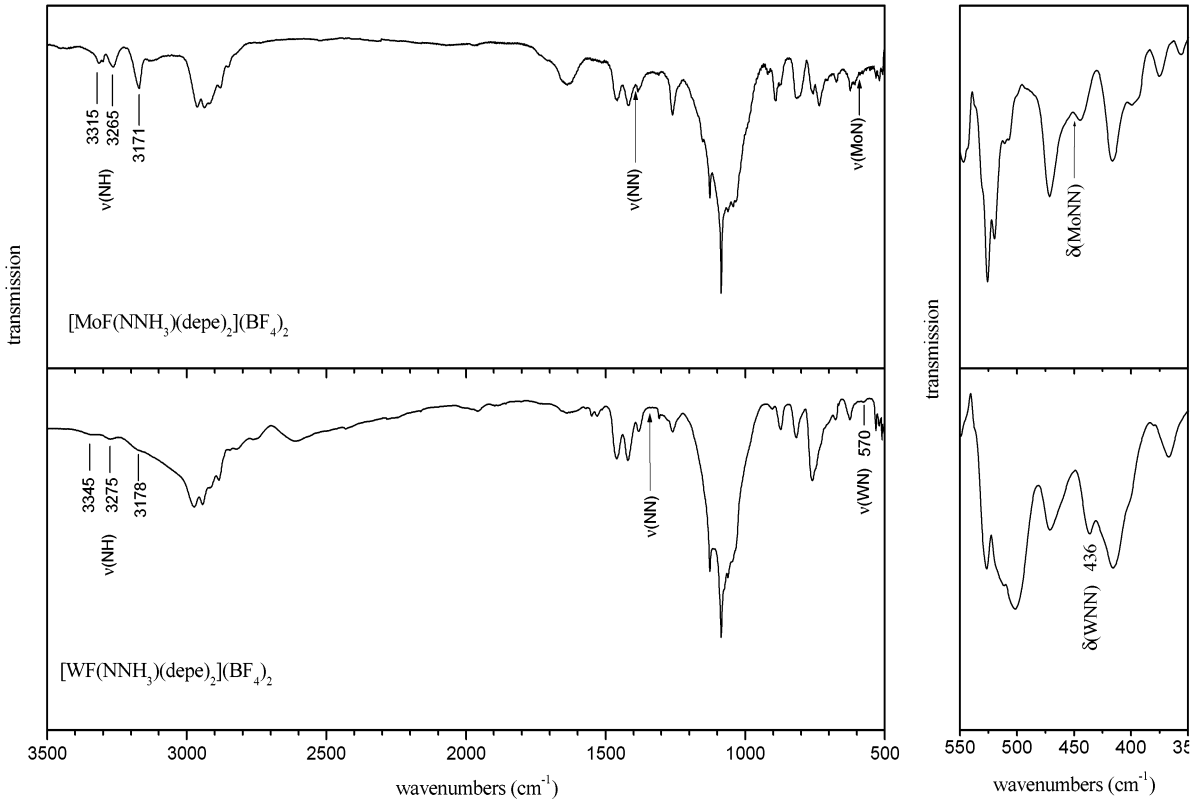

Figure 1. IR spectra of $[MoF(NNH_3)(depe)_2](BF4)_2$ (**IIIa**) and $[WF(NNH_3)(depe)_2](BF_4)_2$ (**VIa**). Observed peaks (in cm^{-1}) and calculated positions, respectively, are indicated.

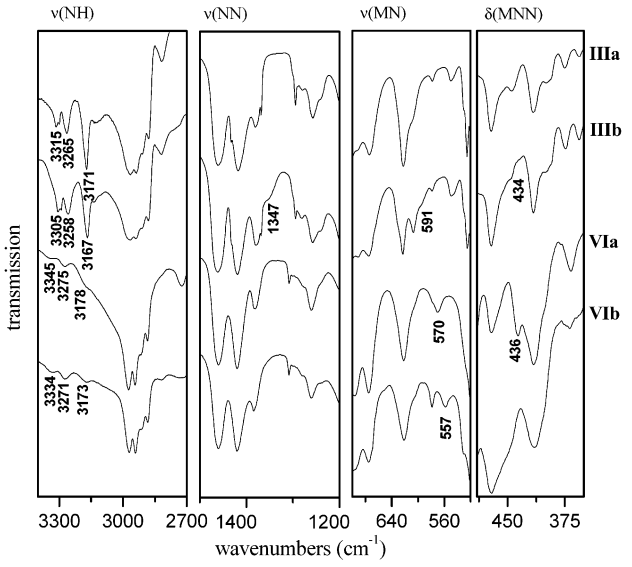

Figure 2. Detail plots showing isotope-sensitive bands in the IR spectra of **IIIa,b** and **VIa,b**.

shift to 3305, 3258, and 3167 cm^{-1}, respectively. The appearance of three N−H vibrations in the IR spectrum unambiguously proves the formation of a hydrazidium complex; corresponding NNH_2 systems only show two sharp bands in this spectral region.[1a]

In the IR spectra of the tungsten systems $[WFNNH_3(depe)_2](BF_4)_2]$ (**VIa,b)**, no peak belonging to ν(NN) can be identified (Figure 2). The three N−H stretching vibrations are now located at 3345, 3275, and 3178 cm^{-1} and shift in the ^{15}N experiment to 3334, 3271, and 3173 cm^{-1}, respectively. The W−N stretch is found at 570 cm^{-1} and upon ^{15}N substitution shifts by about −13 cm^{-1} to 557 cm^{-1}. The feature at 436 cm^{-1} which in the ^{15}N experiment shifts into a broader band at 415 cm^{-1} is assigned to the linear bend δ(WNN). Generally, the metal−N and N−N vibrations are more pronounced in the $W-NNH_3$ spectrum whereas the N−H stretches are much sharper in the $Mo-NNH_3$ complex; both systems therefore provide complementary information.

DFT Frequency Calculation. Besides isotopic substitution and comparison with NNH_2 systems, spectral analysis of the Mo and W hydrazidium compounds is assisted by a DFT frequency calculation on model **IĨI** (see below). This calculation also provides an initial guess for the *f*-matrix which is then used for the normal coordinate analyses (NCA) of compounds **III** and **VI** (QCA-NCA; see below). The three ν(NH) stretching vibrations are calculated by DFT at somewhat higher frequencies than observed in the experiment but qualitatively reproduce the energy splittings and the isotope shifts of these modes (cf. Tables 1 and 2). On the basis of the calculation, the highest-energy vibration is assigned to the totally symmetric stretching mode of the terminal $-NH_3$ moiety (ν_s) whereas the two other bands (ν_s, ν_{as}) are the components of the corresponding antisymmetric N−H vibration (E symmetry in C_{3v}), split by the C_s symmetry of the complex. Specifically, the band at medium energy corresponds to the antisymmetric NH stretch that is symmetric with respect to the molecular plane (ν_s) whereas the lowest-energy band corresponds to the NH vibration that is

Table 1. Comparison of the Observed and Calculated Frequencies of $[MoF(NNH_3)(depe)_2](BF_4)_2$ and $[MoF(^{15}N^{15}NH_3)(depe)_2](BF_4)_2$ in cm^{-1}

	exptl			QCA-NCA			
	NNH_3	$^{15}N^{15}NH_3$	obsd shift	NNH_3	$^{15}N^{15}NH_3$	calcd shift	B3LYP for **IĨI**
ν_s(NH)	3315	3305	−10	3316	3304	−12	3464
ν_s(NH)	3265	3258	−7	3264	3257	−7	3392
ν_{as}(NH)	3171	3167	−4	3170	3168	−2	3312
ν(NN)	n.o	1347		1386	1341	−45	1266
ν(MoN)	n.o	591		593	587	−6	510
ν(MoF)	n.o	n.o		630	621	−9	617
δ(MoNN)	n.o.	434		445	434	379	
				362			

Table 2. Comparison of the Observed and Calculated Frequencies of $[WF(NNH_3)(depe)_2](BF_4)_2$ and $[WF(^{15}N^{15}NH_3)(depe)_2](BF_4)_2$ in cm^{-1}

	exptl			QCA-NCA			
	NNH_3	$^{15}N^{15}NH_3$	obsd shift	NNH_3	$^{15}N^{15}NH_3$	calcd shift	B3LYP for **IĨI**
ν_s(NH)	3345	3334	−11	3344	3331	−13	3464
ν_s(NH)	3275	3271	−4	3278	3271	−7	3392
ν_{as}(NH)	3178	3173	−5	3176	3174	−2	3312
ν(NN)	n.o.	n.o.		1341	1305	−36	1266
ν(WN)	570	557	−13	569	557	−12	510
ν(WF)	n.o.	n.o.		590	588	−2	617
δ(WNN)	436	n.o.		436	424	−12	379
				362			

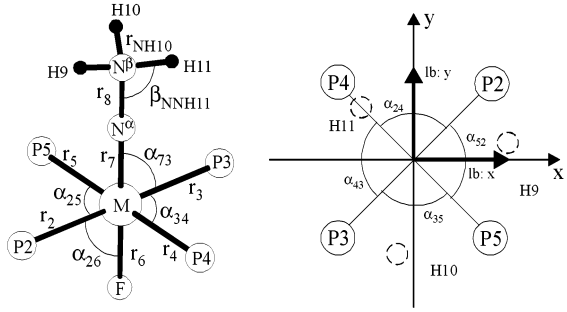

Figure 3. Structure of the model systems $[MF(NNH_3)P_4]^{2+}$, **III′** (M = Mo) and **VI′** (M = W), used for QCA-NCA giving internal coordinated designations and the coordinate system.

antisymmetric with respect to this plane (ν_{as}). The NN− stretch is calculated to be at 1266 cm^{-1}, considerably lower than observed in the Mo system (1347 cm^{-1} in **IIIb**; i.e., at about 1390 cm^{-1} in **IIIa**). The metal−N stretch which is found at 591 cm^{-1} for **IIIb** and at 570/557 cm^{-1} for **VIa/b** is calculated to be at 510 cm^{-1}. Due to the C_s symmetry of the model complex **III′**, a splitting of the doubly degenerate bending mode into two bands at 379 and 362 cm^{-1} (^{14}N) is predicted whereas only one signal at 434 and 436 cm^{-1} is identified for **IIIb** and **VIa**, respectively. The discrepancies between calculated and observed frequencies are ascribed to solid-state effects distorting the gas-phase equilibrium structure, i.e., packing effects and/or hydrogen bridges between the NH_3 group of the hydrazidium ligand and the anions. The metal−F stretch cannot be identified in the spectra of **III** and **VI** but is calculated by DFT to be at 617 cm^{-1}.

Normal Coordinate Analysis. The QCA-NCA procedure is performed as described in the Experimental Section. The structure of the simplified model **III′** $[MF(NNH_3)(P_4)]$ (M = Mo, W) with the internal coordinates used for normal coordinate analysis is given in Figure 3. The corresponding F−M−N−NH_3 core has 15 normal modes: 6 stretches ν_s(MF), ν(MN), ν(NN), 2 ν_s(NH), ν_{as}(NH); 3 N−N−H bends δ(NNH); 3 H−N−H bends δ(HNH); 1 doubly degenerate linear bend δ^{xy}(MNN); 1 torsion τ around the N−N bond which is at very low frequency. Chart 1 shows the symbolic *f*-matrix of the F−Mo−N−NH_3 core. Experimentally determined frequencies are compared to the values determined by QCA-NCA and DFT calculations (B3LYP) in Tables 1 and 2. Force constants resulting from the QCA-NCA procedure are presented in Table 3; their designations correspond to Chart 1.

Chart 1. Symbolic *f*-Matrix of the F−M−N−NH_3 Core of the Models **III′** and **VI′** in C_s Symmetry

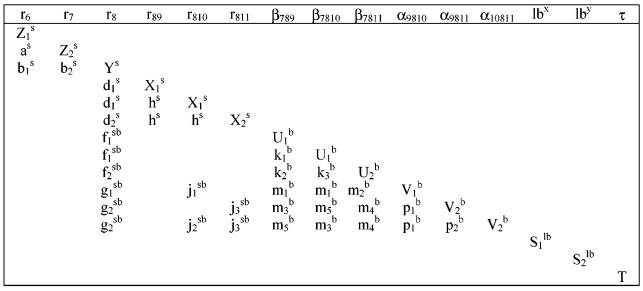

Application of the QCA-NCA procedure to the F−M−N−N unit of the hydrazidium complexes **III** and **VI** is complicated by the fact that no metal−F stretching frequencies are observed. The force constant of the metal fluorine stretch (Z_1^s) is therefore substituted by the B3LYP value (3.62 mdyn/Å; cf. Table 3) and fixed.[19] The structure of the adjacent *f*-matrix is shown in Chart 2 (cf. Chart 1).

In the case of the Mo compound **III**, both ν(NN) and ν(MN) are observable, allowing one to determine diagonal as well as the off-diagonal force constants. This way, the N−N force constant Y^s is determined to 6.03 mdyn/Å, the

(19) The reliability of the DFT prediction of Mo−F frequencies was checked by calculating the Mo−F force constant of MoF_6. Using the identical model chemistry as applied to **III** and **VI** (B3LYP, LANL2DZ), a Mo−F force constant of this molecule was calculated to 4.69 mdyn/Å, in very good agreement with the experimental value (GVFF force constant 4.79 mdyn/Å; see: Labonville, P.; Ferraro, J. R.; Basile, L. J *Coord. Chem. Rev.* **1972**, *7*, 257).

Table 3. Force Constants for $[MF(NNH_3)(depe)_2](BF_4)_2$ (M = Mo, W; Units mdyn/Å for Stretching and mdyn Å for Bending Interactions)

force const	M = Mo	M = W	force const	M = Mo	M = W
Z_1^s	3.62[a]	3.62[a]	b_2^s	0.42	0.42[a]
Z_2^s	8.01	7.31	d_1^s	0.18[a]	0.18[a]
Y^s	6.03	6.03[b]	d_2^s	0.18[a]	0.18[a]
X_1^s	5.83	5.89	f_1^{sb}	0.22[a]	0.22[a]
X_2^s	5.92	5.97	f_2^{sb}	0.22[a]	0.22[a]
U_1^b	0.62	0.62[b]	g_1^{sb}	−0.23[a]	−0.23[a]
U_2^b	0.62	0.62[b]	g_2^{sb}	−0.23[a]	−0.23[a]
V_1^b	0.59	0.59[b]	j_1^{sb}	0.06[a]	0.06[a]
V_2^b	0.58	0.58[b]	j_2^{sb}	0.11[a]	0.11[a]
S_1^{lb}	0.63	0.65	j_3^{sb}	0.12[a]	0.12[a]
S_2^{lb}	0.63	0.65	k_2^b	−0.14[a]	−0.14[a]
T	0.002[a]	0.002[a]	m_1^b	−0.10[a]	−0.10[a]
a^s	0.78	0.78[b]	m_2^b	−0.15[a]	−0.15[a]
b_1^s	0.076[a]	0.076[a]	m_3^b	−0.10[a]	−0.10[a]
h^s	0.0	−0.04	m_4^b	−0.10[a]	−0.10[a]
k_1^b	−0.14	−0.14[b]	m_5^b	−0.15[a]	−0.15[a]
p_2^b	−0.12	−0.12[b]	p_1^b	0.11[a]	0.11[a]

[a] Taken from DFT and fixed. [b] Taken from the Mo calculation and fixed.

Chart 2

	M-F	M-N	N-N	
M-F	Z_1^s			
M-N	a^s	Z_2^s		
N-N	b_1^s	b_2^s	Y^s	

Mo−N force constant Z_2^s is determined to 8.01 mdyn/Å, and values for a^s of 0.42 mdyn/Å and for b_2^s of 0.78 mdyn/Å are obtained. The off-diagonal matrix element b_1^s describing the coupling between M−F and N−N is small; therefore, the DFT value (0.076 mdyn/Å) is used and fixed. In the case of the F−W−N−N unit of compound **VI**, only the metal−N stretch is observable. Therefore, the above matrix elements of the Mo compound **III** are adapted, only adjusting Z_2^s to fit the experimentally observed W−N frequencies (see below). This gives $Z_2^s = 7.31$ mdyn/Å, somewhat lower than the value for **III**. For the Mo−NN and W−NN linear bends, force constants of 0.63 and 0.65 mdyn Å, respectively, are obtained. NH-stretching force constants are fitted to $X_1^s = 5.83$ mdyn/Å and $X_2^s = 5.92$ mdyn/Å for **III** and $X_1^s = 5.89$ mdyn/Å and $X_2^s = 5.97$ mdyn/Å for **VI**, respectively.

Agreement between the experimental frequencies and the results of QCA-NCA is good (Tables 1 and 2). The NN stretch is calculated at 1341 cm^{-1} for the ^{15}N-substituted Mo−NNH_3 compound which is close to the frequency of 1347 cm^{-1} observed for **IIIb**; the predicted isotope shift for this vibration is 45 cm^{-1}. ν(MoN) is calculated at 593 cm^{-1} and predicted to shift to 587 cm^{-1} upon isotopic substitution (measured for **IIIb**: 587 cm^{-1}) while for the Mo−F stretching vibration a frequency of 630 cm^{-1} with an isotope shift of −9 cm^{-1} results. The ν(WN) mode which is observed at 570 (**VIa**) and 557 cm^{-1} (**VIb**) is very well reproduced at 569 and 557 cm^{-1}, respectively; for ν(WF) frequencies of 590 (^{14}N) and 588 cm^{-1} (^{15}N) are predicted. The metal−NN bending modes of **III** are calculated by QCA-NCA at 445 cm^{-1} with a ^{15}N shift of −11 cm^{-1}, which is compatible to the ^{15}N spectrum of **III** where one δ(MoNN) vibration is found at 434 cm^{-1}. The δ(WNN) vibration of **VIa** is calculated by QCA-NCA at 436 cm^{-1}, the experimental value, giving the following ^{15}N shift: −12 cm^{-1}. Finally, the NH streching frequencies of **III** and **VI** and their isotopic shifts show excellent agreement with the observed values.

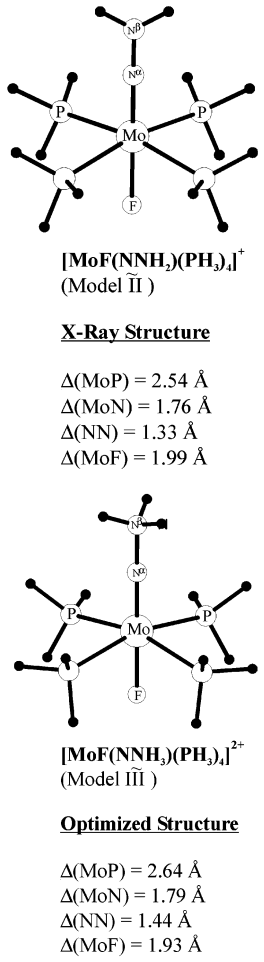

Figure 4. Structures of the model complexes **ĨI** and **IĨĨ** used for DFT calculations.

2. Electronic Structure.

Input Geometries and Structure Optimizations. The structure of the NNH_2 model system $[MoF(NNH_2)(PH_3)_4]^+$ (**ĨI**) is derived from the crystal structure of $[MoF(NNH_2)(dppe)_2](BF_4)$[20] and not optimized. The complete electronic structure of **ĨI** has been presented before;[1b] here, model **ĨI** is only used for time-dependent DFT (TDDFT) calculations to assign the transition energies observed in optical absorption spectra of compounds **II** and **V** (see the following section). By addition of a third hydrogen atom at a N−H distance known from the NNH_2 complex and performance of a full geometry optimization, model system **IĨĨ** is obtained (see below).

Frontier Orbitals of the Free Ligand. Bonding of three protons to N_2 and four-electron transfer generate NNH_3^- species (hydrazidium). Loss of coupling between the p orbitals of the coordinating and the terminal nitrogen of N_2 which is already observed in the NNH and NNH_2 species[1b]

(20) Hidai, M.; Kodama, T.; Sato, M.; Harakawa, M.; Uchida, Y. *Inorg. Chem.* **1976**, *15*, 2694.

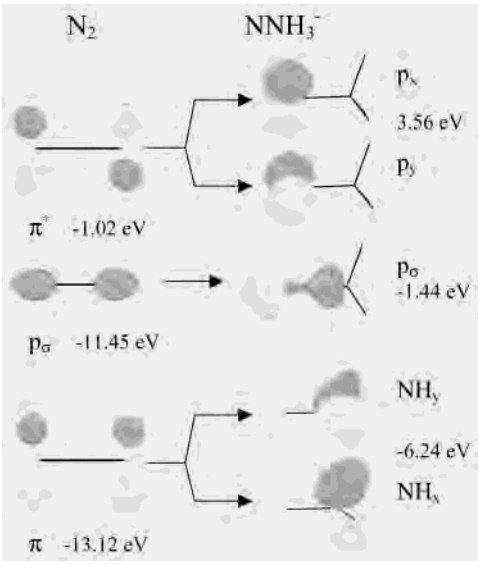

Figure 5. Frontier orbitals of the free ligands N_2 and NNH_3^-. Orbital energies are indicated.

Table 4. Comparison of Experimental and Calculated Structures for Model **IĨI**

		M−P	M−N	N−N	M−X	N−H
$[MoF(NNH_3)(PH_3)_4]^{2+}$	opt	2.64	1.79	1.44	1.93[a]	1.04
$[WCl(NNH_3)(PMe_3)_4]Cl_2$	X-ray	2.519	1.785	1.396	2.463[b]	

[a] Mo−F. [b] W−Cl.[7]

is further proceeding; i.e., the vertical (π_x) and horizontal (π_y) π orbitals of N_2 are now transformed into two NH bonding orbitals on N^β whereas the two degenerate π^* orbitals of dinitrogen have evolved into two orbitals p_x and p_y mostly having lone pair character at the coordinating nitrogen N^α (Figure 5). N−N bonding is mediated by the orbital p_σ; the N−N triple bond of N_2 is therefore reduced to a single σ bond.

Electronic Structure of the Mo−NNH$_3$ Complex (IĨI). The structure of the NNH_3 model system $[MoF(NNH_3)(PH_3)_4]^{2+}$ (**IĨI**) is given in Figure 4. The optimized structure parameters as well as a comparison with the data from a single-crystal analysis of $[WCl(NNH_3)(PMe_3)_4]Cl_2$[8] are given in Table 4. Addition of three H^+ to complex **I** leading to the triply protonated species **III** causes a shortening of the Mo−N bond and an enlargement of the NN bond; i.e., the Mo−N distance is reduced from 2.014 Å in model **Ĩ** of the dinitrogen complex[1b] to 1.79 Å in the NNH_3 complex **IĨI**, whereas the N−N distance is elongated from 1.164 to 1.44 Å.

The MO diagram of **IĨI** along with contour plots of important orbitals is shown in Figure 6; orbital compositions are given in Table 5. The HOMO of **IĨI** is the nonbonding orbital d_{xy} which, in comparison to the NNH_2 complex, is shifted to lower energies. Below the HOMO are the bonding combinations of d_{xz} and d_{yz} with the NNH_3 p-donor orbitals p_x and p_y, corresponding to two M−N π bonds. These MO's are denoted as $p_x\_d_{xz}$ and $p_y\_d_{yz}$ (or simply p_x and p_y) and have 45% N_2, 16% P, and 18% Mo contribution. Metal−ligand σ bonding is mediated by $p_\sigma\_d_{z^2}$. Bonding in the equatorial ligand sphere is dominated by orbital $P\_d_{x^2-y^2}$ with

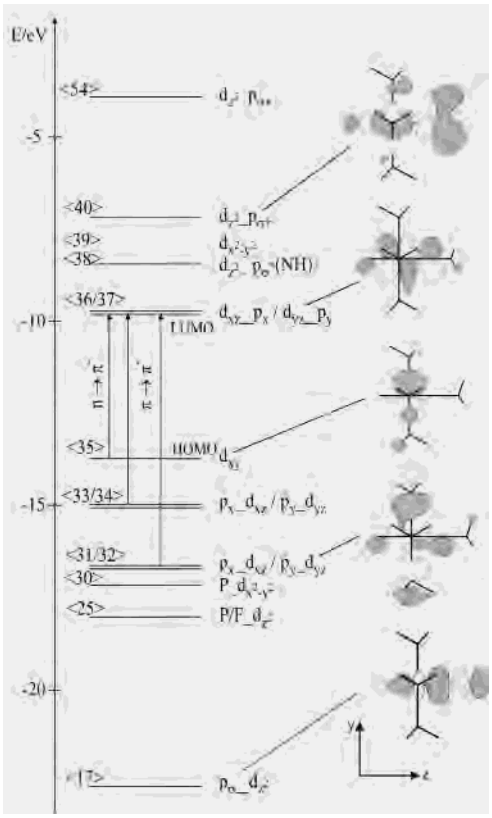

Figure 6. MO diagram and contour plots of important molecular orbitals of **IĨI** along with prominent optical transitions.

Table 5. Charge Contributions of $[MoF(NNH_3)(PH_3)_4]^{2+}$ (**IĨI**)

			orbital composns (%)						
orbital	label	energy (eV)	Mo	P	F	N1	N2	H^N	H^P
$d_{z^2}\_p_{\sigma^*}$	a′⟨54⟩	−3.9348	33	6	1	20	35	4	1
$d_{z^2}\_p_{\sigma^*}$	a′⟨40⟩	−7.2056	17	11	3	28	17	17	3
$d_{x^2-y^2}$	a′⟨39⟩	−8.0165	35	62	0	0	0	0	2
$d_{z^2}\_p_{\sigma^*}$ (NH)	a′⟨38⟩	−8.4764	25	11	1	4	42	14	2
$d_{xz}\_p_x$	a″⟨37⟩	−9.8179	55	1	6	24	1	9	3
$d_{yz}\_p_y$	a′⟨36⟩	−9.8260	55	1	6	24	1	9	3
d_{xy}	a″⟨35⟩[a]	−13.7608	88	0	0	0	0	0	12
$p_x\_d_{xz}$	a″⟨34⟩[a]	−15.0806	7	51	14	20	0	1	6
$p_y\_d_{yz}$	a′⟨33⟩[a]	−15.0860	7	51	14	20	0	1	6
$p_x\_d_{xz}$	a″⟨32⟩[a]	−16.7432	18	16	10	43	2	3	8
$p_y\_d_{yz}$	a′⟨31⟩[a]	−16.7432	18	16	10	43	2	3	8
P_d_{x2-y2}	a″30′*	−17.1894	48	43	0	0	0	0	9
F(p)	a″⟨29⟩[a]	−17.4969	12	10	61	3	0	0	13
F(p)	a′⟨28⟩[a]	−17.5105	12	10	62	3	0	0	12
F(p)	a″27′*	−17.5514	9	8	67	9	2	0	3
PH_3	a″⟨26⟩[a]	−17.9568	0	46	1	0	0	0	53
$P/F\_d_{z^2}$	a′⟨25⟩[a]	−18.0520	29	38	16	4	1	0	11
$p_\sigma\_d_{z^2}$	a′⟨17⟩[a]	−22.6426	18	0	4	49	4	1	0

[a] Occupied orbitals.

48% $d_{x^2-y^2}$ and 43% phosphine contribution. The LUMO is part of a 2-fold degenerate set of the antibonding combinations $d_{xz}\_p_x$ and $d_{yz}\_p_y$, also simply denoted as d_{xz}/d_{yz}, which predominantly have metal character (55%). To higher energy the antibonding combinations of d_{z^2} with p_σ are found. They split into three orbitals with variable metal and N−H contributions.

On the basis of this MO scheme, the NNH_3 ligand has a single N−N σ bond and is coordinated to the metal center by a metal−N triple bond. The metal has a d^2 electronic

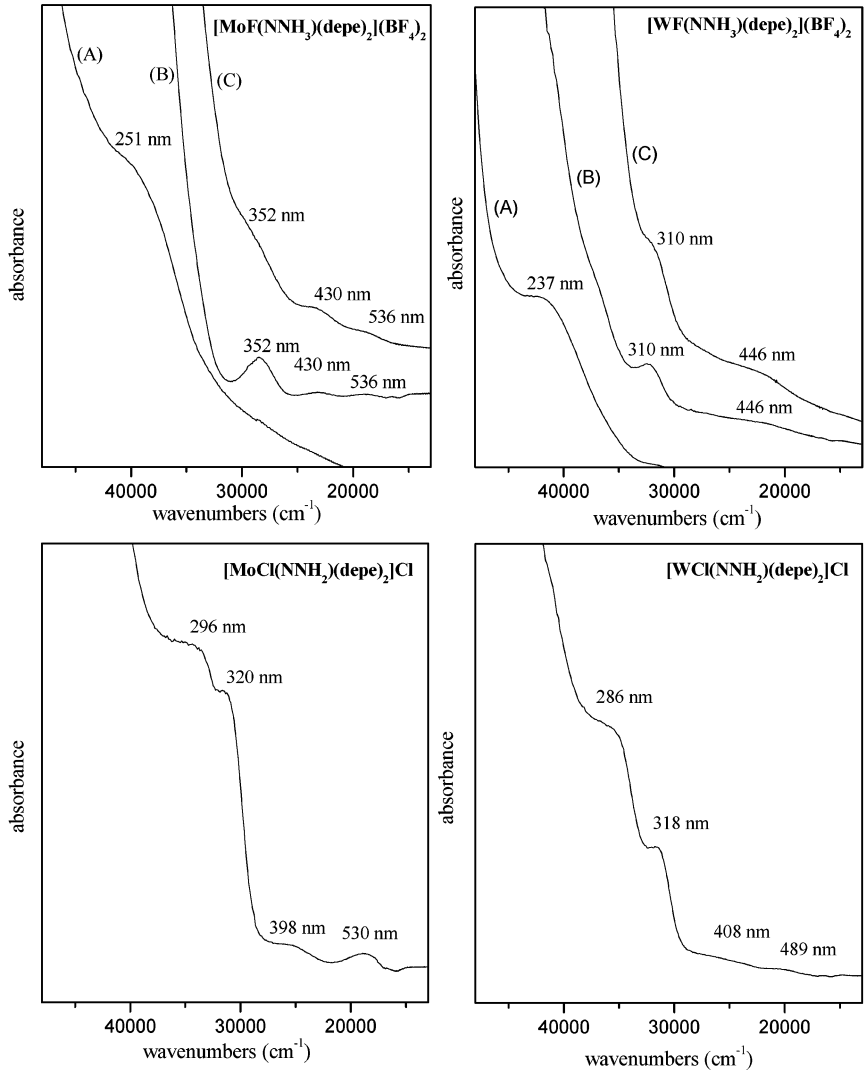

Figure 7. Solid-state optical absorption spectra of **III** (top left), **VI** (top right), **II** (bottom left), and **V** (bottom right): (A) KBr pellet at room temperature; (B) neat complex pressed between sapphire windows at 10 K; (C) concentrated KBr pellet at 10 K; **II** and **V** neat complexes.

Table 6. NPA Charges of $[MoF(NNH_3)(PH_3)_4]^{2+}$

Mo	N^{α}	N^{β}	H_N	H'_N	F	PH_3	PH_3'	PH_3''
0.19	−0.36	−0.60	0.48	0.48	−0.44	0.44	0.44	0.44

configuration with two electrons being in the nonbonding d_{xy} orbital and therefore is assigned a formal +IV oxidation number. As evident from the NPA (natural population analysis) charges (Table 6), the electronic charge on the NNH_3 ligand is reduced from (formally) −1 to +0.48; i.e., this ligand donates about 1.5 charge units to the metal(IV) center. From Table 6, this charge is mostly withdrawn from the coordinating "imido" $(N^{\alpha})^{2-}$ atom whereas the terminal $-N^{\beta}H_3$ group carries a charge of about +1. The +4 formal charge of the Mo center is further reduced by donation from F^- (0.56) and the phosphine ligands (4 × 0.44), leading to an effective charge of +0.19 (Table 6).

3. Electronic Spectroscopy.

NNH_3 Complexes of Mo and W. Figure 7, top left, shows solid-state absorption spectra of the Mo−NNH_3 complex **III**. Four bands at 536, 430, 352, and 251 nm can be identified. In the spectrum of the tungsten analogue **VI** (Figure 7, top right), only three absorption bands at 446, 310, and 237 nm are found. Time-dependent DFT (TDDFT) has been employed to assign these features; Table 7 collects the observed band positions as well as the lowest 10 transitions obtained from TDDFT on model **IĨI**. Band assignments are based on the agreement between theoretical and measured transition energies. The ligand-field transitions originating from the HOMO are $d_{xy} \rightarrow d_{xz}\_p_x/d_{yz}\_p_y$ (HOMO → LUMO ($n \rightarrow \pi^*$) transitions) as well as $d_{xy} \rightarrow d_{x^2-y^2}$ and $d_{xy} \rightarrow d_{z^2}$; TDDFT predicts vanishing or very small intensities for all of these features. For compound **III**, the HOMO−LUMO transition is observed at 536 nm (18 657 cm^{-1}) and calculated at 17 830 cm^{-1}; for compound **VI** this transition is not observed. The transition to $d_{x^2-y^2}$ is observed at 446 nm (23 256 cm^{-1}) for **III** and 430 nm (22 422 cm^{-1}) for **VI**; the calculation predicts this transition at somewhat higher energy (23 976 cm^{-1}). $d_{xy} \rightarrow d_{z^2}$ is calculated at 29 267 cm^{-1} and found at 310 nm (28 409 cm^{-1}; **III**) and 352 nm (32 358 cm^{-1}; **VI**), respectively. This absorption band is more intense than the lower-energy LF transitions which, however, is not reflected in its calculated intensity. An excitation energy of 38 456 cm^{-1} is

Table 7. Calculated[a] and Experimental Transition Energies for $[MF(NNH_3)(depe)_2](BF_4)_2$

calcd (cm^{-1})	exptl (cm^{-1}) M = Mo	exptl (cm^{-1}) M = W	state	assgnt	oscillator strength
17 823	18 657		a″	$d_{xy} \rightarrow d_{yz}\_p_y$	0.0001
17 835			a′	$d_{xy} \rightarrow d_{xz}\_p_x$	0.0001
23 976	23 256	22 422	a″	$d_{xy} \rightarrow d_{x^2-y^2}$	0.0
29 267	28 409	32 258	a″	$d_{xy} \rightarrow d_{z^2}$	0.0
34 183			a′	$p_y \rightarrow d_{yz}/p_x \rightarrow d_{xz}$	0.0
35 177			a′	$p_y \rightarrow d_{yz}/p_x \rightarrow d_{xz}$	0.0
35 349			a″	$p_y \rightarrow d_{xz}/p_x \rightarrow d_{yz}$ $d_{xy} \rightarrow d_{z^2}$	0.0
38 456	39 841	42 194	a″	$p_y \rightarrow d_{xz}/p_x \rightarrow d_{yz}$	0.0109
41 639			a′/a″	$p_y \rightarrow d_{yz}/p_y \rightarrow d_{xz}/p_x \rightarrow d_{yz}/p_x \rightarrow d_{xz}$	0.0
41 829			a′/a″	$p_y \rightarrow d_{yz}/p_y \rightarrow d_{xz}/p_x \rightarrow d_{yz}/p_x \rightarrow d_{xz}/d_{xy} \rightarrow d_{z^2}$	0.0002

[a] Calculated for the model **IĨI**.

Table 8. Calculated[a] and Experimental Transition Energies for $[MCl(NNH_2)(depe)_2]Cl$

calcd (cm^{-1})	exptl (cm^{-1}) M = Mo	exptl (cm^{-1}) M = W	state	assgnt[b]	oscillator strength
19 719	18 868	20 450	b_2	$d_{xz} \rightarrow d_{x^2-y^2}/d_{xy} \rightarrow d_{yz}$	0.0002
23 603			a_2	$d_{xz} \rightarrow d_{yz}/d_{xy} \rightarrow d_{x^2-y^2}$	0.0
24 688			a_2	$d_{xz} \rightarrow d_{yz}/d_{xy} \rightarrow d_{x^2-y^2}$	0.0
27 015	25 126	24 510	b_1	$d_{xy} \rightarrow \pi^*_v$	0.001
33 331			b_2	$d_{xz} \rightarrow d_{x^2-y^2}$	0.002
33 629	31 250	31 447	a_1	$\pi^*_h \rightarrow d_{yz}/d_{xz} \rightarrow \pi^*_v/d_{xy} \rightarrow d_{z^2}$	0.0119
36 451	33 784	34 965	a_1	$\pi^*_h \rightarrow d_{yz}/d_{xz} \rightarrow \pi^*_v/d_{xy} \rightarrow d_{z^2}$	0.0192
37 933			b_1	$d_{xz} \rightarrow d_{z^2}$	0.0082
41 890			b_2		0.0171
42 107			a_1	$\pi^*_h \rightarrow d_{yz}$	0.0006

[a] Calculated for the model **IĨ**. [b] See text.

calculated for the $p_x \rightarrow d_{xz}$ and $p_y \rightarrow d_{yz}$ ($\pi \rightarrow \pi^*$) transitions; in the spectra the corresponding absorptions are found at 251 nm (39841 cm^{-1}) for compound **III** and 237 nm (42194 cm^{-1}) for **VI**, respectively.

NNH_2 Complexes of Mo and W. For comparison, optical absorption spectra of the NNH_2 complexes **II** (Mo) and **V** (W) have been recorded (Figure 7, bottom). In these systems the π^* orbitals split into one orbital in the NNH_2 plane (π^*_h) and one perpendicular to it (π^*_v) and the metal has four electrons in d_{xz} and d_{xy}.[1b] The Mo spectrum (left) exhibits two weak absorption bands at 530 and 398 and two strong bands 320 and 296 nm; the W spectrum (right) is qualitatively similar. Assignments using the results of TDDFT calculations on model **ĨI** are presented in Table 8. The $d_{xy} \rightarrow d_{yz}$ transition is observed in the spectra at 530 nm (18 868 cm^{-1}; **II**) and 489 nm (20 450 cm^{-1}; **V**), respectively (calculated transition energy: 19 719 cm^{-1}), whereas the $d_{xy} \rightarrow \pi^*_v$ transition is found at 398 nm (25 126 cm^{-1}) in the spectrum of **II** and at 408 nm (24 510 cm^{-1}) in the spectrum of **V**, respectively (calculated transition energy: 27 027 cm^{-1}). At 320/296 nm (31 250/33 784 cm^{-1}) in the spectrum of **II** and at 318/286 nm (31447/34965 cm^{-1}) in the spectrum of **V**, the higher-intensity $\pi \rightarrow \pi^*$ transitions $\pi^*_h \rightarrow d_{yz}$ and $d_{xz} \rightarrow \pi^*_v$ are observed. These transitions are calculated at 33 629 and 36 451 cm^{-1}, respectively. The first transition is in-plane with respect to the NNH_2 unit, and the second one out-of-plane. Importantly, both transitions are at lower energy than observed for the hydrazidium compounds **III** and **VI**, in agreement with the lower metal−ligand covalency in the NNH_2 as compared to the NNH_3 system.

Discussion

The investigations presented in the preceding sections have led to a spectroscopic and electronic−structural characterization of Mo and W hydrazidium (NNH_3^-) complexes. Such systems play a critical role in the end-on terminal reduction pathway of N_2 to NH_3 as they represent the highest level of N_2 protonation in this reaction mode and the last intermediate before the splitting of the N−N bond.

In the dinitrogen chemistry of Mo and W, octahedral hydrazidium complexes only form under special conditions. So far, they have exclusively been isolated as tungsten systems with mono- and bidentate phosphine coligands carrying terminal alkyl groups, being generated from the corresponding bis(dinitrogen) complexes of W(0) by protonation with HBF_4 or HCl.[7,8] These acids introduce a fluoro and a chloro ligand in a trans position to the NNH_3 group, respectively. In contrast, protonation of Mo and W bis(dinitrogen) complexes having bidentate phosphine ligands with aromatic groups (dppe) was found to only lead to NNH_2 complexes.[21] Protonation of bis(dinitrogen) systems with monodentate mixed aryl/alkyl phosphine ligands, finally, generates NH_3 under decomposition of the metal−phosphine complex.[22] On the basis of our interest in a well-defined reduction pathway of N_2 mediated by Mo/W complexes with

(21) (a) Jimenez-Tenorio, M.; Puerta, M. C.; Valerga, P.; Hughes, D. L. *J. Chem. Soc., Dalton Trans.* **1994**, 2431. (b) George, T. A.; Kaul, B. B.; Chen, Q.; Zubieta, J. *Inorg. Chem.* **1993**, *32*, 1706. (c) George, T. A.; Ma, L.; Shailh, S. N.; Tisdale, R. C.; Zubieta, J. *Inorg. Chem.* **1990**, *29*, 4789. (d) Galindo, A.; Hills, A.; Hughes, D. L.; Richards, R. L.; Hughes, M.; Mason, J. *J. Chem. Soc., Dalton Trans.* **1990**, 283. (e) Barclay, J. E.; Hills, A.; Hughes; D. L.; Leigh, G. J.; Macdonald, C. J.; Abu Bakar, M.; Mohd-Ali, H. *J. Chem. Soc., Dalton Trans.* **1990**, 2503 (f) Abu Bakar, M.; Hughes, D. L.; Hussain, W.; Leigh, G. J.; Macdonald, C. J.; Mohd-Ali, H. *J. Chem. Soc., Dalton Trans.* **1988**, 2545. (g) George, T. A.; Tisdale; R. C. *J. Am. Chem. Soc.* **1985**, *107*, 5157. (h) Chatt, J.; Fakley, M. E.; Hitchcock, P. B.; Richards, R. L.; Luong-Thi, N. T. *J. Chem. Soc., Dalton Trans.* **1982**, 345. (i) Takahasi, T.; Mizobe, Y.; Sato, M.; Uchida, Y.; Hidai, M. *J. Am. Chem. Soc.* **1980**, *102*, 7461. (j) Chatt, J.; Pearman, A. J.; Richards, R. L. *J. Chem. Soc., Dalton Trans.* **1978**, 1766. (k) Chatt, J.; Pearman, A. J.; Richards, R. L. *J. Chem. Soc., Dalton Trans.* **1977**, 2139 (l) Chatt, J.; Pearman, A. J.; Richards, R. L. *J. Chem. Soc., Dalton Trans.* **1977**, 1852. (m) Chatt, J.; Pearman, A. J.; Richards, R. L. *J. Chem. Soc., Dalton Trans.* **1976**, 1520. (n) Heath, G. A.; Mason, R.; Thomas, K. M. *J. Am. Chem. Soc.* **1974**, *96*, 260. (o) Chatt, J.; Heath, G. A.; Richards, R. L. *J. Chem. Soc., Dalton Trans.* **1974**, 2074. (p) Chatt, J.; Heath, G. A.; Richards, R. L. *J. Chem. Soc., Chem. Commun.* **1972**, 1010.

(22) Chatt, J.; Pearman, A. J.; Richards, R. L. *J. Am. Chem. Soc.* **1977**, *99*, 2.

a robust equatorial P_4 coordination, we investigated the known W−NNH_3 system [$WF(NNH_3)(depe)_2$](BF_4)$_2$ (**VI**) using vibrational spectroscopy (IR/Raman) and DFT calculations. In addition, we succeeded preparing the analogous complex [$MoF(NNH_3)(depe)_2$](BF_4)$_2$ (**III**) the spectroscopic properties of which are compared to its tungsten counterpart. This continues our line of research which has started with an investigation of the electronic structure and the spectroscopic properties of Mo/W−N_2, N_2H, and N_2H_2 complexes.[1]

Upon triple protonation of the N^{β} atom of coordinated N_2, the doubly degenerate sets of dinitrogen π and π^* orbitals evolve into doubly degenerate sets of NH bonding orbitals on N^{β} and lone pairs on N^{α}, respectively (Figure 5). Population of these orbitals requires four additional electrons which are transferred from the W(0) or Mo(0) d^6 central atom of the parent N_2 complex to the NNH_3 unit, leaving the metal in a +IV oxidation state (d^2 configuration). The NNH_3 ligand thus formally acquires one negative charge (NNH_3^-), and the N−N triple bond of N_2 is reduced to a single σ bond between N^{α} and N^{β}. Conversely, σ interaction between the hydrazidium ligand and the metal d_{z^2} orbital along with π interaction between the lone pairs of N^{α} and the metal d_{xz}/d_{yz} orbitals form a triple bond between NNH_3 and the metal(IV) center. By ligand → metal σ and π donation, about 1.5 negative charge units are transferred from the ligand back to the metal center. Metal−ligand bonding in NNH_3 complexes is thus analogous to nitrido, imido, or oxo compounds.[23]

This bonding scheme is supported by the results of vibrational spectroscopy. The N−N force constant of **III** and **IV** is determined to 6.03 mdyn/Å, and the metal−N force constants are determined to 8.01 (Mo−N) and 7.31 mdyn/Å (W−N), respectively. While the metal−N force constants are similar to those of analogous Mo(IV) nitrido or imido complexes (f(Mo−N) = 8.09 and 7.68 mdyn/Å, respectively),[24] the N−N force constant is higher than found for the N−N single bond in hydrazine. However, with comparison of the N−N bond length of hydrazine (1.46 Å)[25] with the relatively short N−N bond length of the NNH_3 complex (from the crystal structure of [$WCl(NNH_3)(PMe_3)_4$]Cl_2, d(N−N)=1.396 Å)[8] and application of Badger's rule,[26] the N−N force constant of hydrazine (4.3 mdyn/Å)[27] should be increased in the W−NNH_3 compound to 5.6 mdyn/Å, reasonably close to the value of 6.03 mdyn/Å determined for **III** and **VI**. Importantly, this N−N force constant shows a further decrease with respect to the values of 8.27 and 7.20 mdyn/Å found for the NNH− and the NNH_2 complex, respectively.[1] Conversely, the metal−N force constants in the hydrazidium complexes (8.01 and 7.31 mdyn/Å, respectively) show a further increase from the value of 4.50 mdyn/Å observed for the NNH− and 6.31 mdyn/Å observed for the NNH_2 complex, respectively. The evolution of N−N force constants upon successive protonation indicates a stepwise decrease in N−N bond strength initiating bond cleavage whereas the evolution of metal−N force constants reflects an increase of metal−ligand covalency, indicative of a successive strengthening of the metal−N bond. This provides an energetic driving force for the reduction of the N−N triple bond and acts to prevent loss of partly reduced NNH_x substrate, $x = 1-3$.

The bonding scheme established for the Mo and W hydrazidium complexes is further supported by optical absorption spectroscopy on complexes **III** and **VI** coupled to time-dependent DFT (TDDFT) calculations on a Mo−NNH_3 model system. The (metal−ligand)$\pi \rightarrow \pi^*$ optical transition is calculated by TDDFT to 38 456 cm^{-1}, which shows good agreement with absorption bands at 251 nm (39 841 cm^{-1}, **III**) and 237 nm (42 194 cm^{-1}, **VI**), respectively. The two d electrons of the metal are located in the nonbonding (n) d_{xy} orbital; the n → π^* optical transition is calculated by TDDFT at 17 830 cm^{-1} which compares well with an absorption band at 536 nm (18 657 cm^{-1}, **III**). Higher-energy ligand-field (LF) bands in the optical absorption spectra of **III** and **VI** are assigned to $d_{xy} \rightarrow d_{x^2-y^2}$ (446 nm = 23 256 cm^{-1} for **III**) and $d_{xy} \rightarrow d_{z^2}$ (352 nm = 32 358 cm^{-1} for **III**), respectively. This energetic sequence of LF transitions is in agreement with that found for analogous Mo(IV) oxo compounds with phosphine coligands.[23b]

For comparison, optical absorption spectra of the Mo- and W(NNH_2)$(depe)_2$ complexes **II** and **V**, respectively, have been recorded and interpreted by TDDFT as well. Both LF and $\pi \rightarrow \pi^*$ transition regions of these spectra are markedly different from those of analogous NNH_3 systems. The LF region of the NNH_2 complexes exhibits bands at 398 and 530 nm (**III**; 408 and 498 nm in **V**), which are assigned to the transitions $d_{xy} \rightarrow \pi^*_v$ and $d_{xy} \rightarrow d_{yz}$, respectively. These features are masked in the analogous dppe complexes by a metal → phosphine CT band.[1b] With respect to the corresponding NNH_3 systems, the $\pi \rightarrow \pi^*$ transitions are shifted to lower energy and split into two bands at 320/296 nm (31 250/33 784 cm^{-1}) in **II** and 318/286 (31 447/34 965 cm^{-1}) in **V**. This reflects the lower degree of metal−ligand covalency as compared to the NNH_3 system and the splitting of the ligand π^* orbitals into one orbital within (π^*_v) and one orbital perpendicular to the NH_2 plane (π^*_v), respectively.

As indicated at the beginning, formation of hydrazidium complexes requires strongly electron-donating equatorial phosphine ligands with terminal alkyl groups, employing strong acids in a large excess. Whereas up to now only W−NNH_3 complexes have been isolated and characterized, we found that an analogous molybdenum complex exhibits a comparable stability in the solid state. Generally, crystallization of these species is favored by strong H-bonds stabilizing the NNH_3 ligand. Thermal stability of **III** and **VI** in solution, on the other hand, is limited due to the phosphine ligands becoming labile at this stage of N_2 reduction. This corresponds to a marked tendency of the

(23) (a) Cowman, C. D.; Trogler, W. C.; Mann, K. R.; Poon, C. K.; Gray, H. B. *Inorg. Chem.* **1976**, *15* (8), 1747. (b) Bendix, J.; Bøgevig, A. *Inorg. Chem.* **1998**, *37*, 5992−6001.
(24) Mersmann, K. Diplomarbeit Universität Kiel, 2002 (unpublished).
(25) Sutton, L. E. *Tables of Interatomic Distances and Configuration in Molecules and Ions;* Chemical Society Special Publication No. 11; Chemical Society: London, 1958.
(26) Herschbach, D. R.; Laurie, V. W. *J. Chem. Phys.* **1961**, *35* (2), 458.
(27) Catalano, E.; Sanborn, R. H.; Frazer, J. W. *J. Chem. Phys.* **1963**, *38*, 2265.

Mo−NNH_3 model complex **IĨI** to lose PH_3 groups in the course of the geometry optimization. Loss of phosphine ligands probably is also the origin for the formation of $^{15}NH_3$, which we identified by ^{15}N NMR in solutions of **VIb**, paralleling the much faster NH_3 generation based on the protonation of Mo− and W−N_2 complexes with monodentate mixed alkyl/aryl coligands which proceeds under exchange of phosphine ligands.[22] Maximum thermodynamic stability of the Mo/W complexes at the NNH_3 stage of protonation therefore requires the presence of bidentate phosphine coligands.

To obtain further insight into the stability of **III** and **VI** with respect to the splitting of the N−N bond, the heterolytic N−N cleavage of $[MoF(NNH_3)(PH_3)_4]^{2+}$ (**IĨI**) leading to ammonia and the Mo(VI) nitrido complex $[MoF(N)(PH_3)_4]^{2+}$ was investigated with the help of DFT:[28]

$$[MoF(NNH_3)(PH_3)_4]^{2+} \xrightarrow[A]{} [MoF(N)(PH_3)_4]^{2+} + NH_3 \xrightarrow[B]{H^+} [MoF(N)(PH_3)_4]^{2+} + NH_4^+ \quad (1)$$

Using the same methodology as applied before (B3LYP, LANL2DZ), reaction step A was found to be endothermic ($\Delta H°_A = +41$ kcal/mol, $\Delta G°_A = +31$ kcal/ mol). In strongly acidic media the NH_3 molecule generated in step A is converted to NH_4^+ (reaction step B). An estimate of the free reaction enthalpy of this step is obtained from the protonation of NH_3 in water: on the basis of the pK_a value of NH_4^+ (9.25), the corresponding standard free reaction enthalpy is $\Delta G° = -13$ kcal/mol. The standard free enthalpy $\Delta G°$ of the total reaction 1 including protonation of NH_3 then amounts to $\Delta G° = \Delta G°_A + \Delta G°_B \approx 31-13$ kcal/mol $= 18$ kcal/mol, and the dissociation of the N−N bond represents an activation barrier of this reaction which can be estimated to $\Delta G^‡ = 31$ kcal/mol, the free reaction enthalpy of step A.

The actual activation energy of reaction 1, however, will be much higher than this value, for the following reason: electronically, N−N cleavage is induced by transfer of electron density from the metal d_{xy} orbital into the p_σ* orbital of the NNH_3 ligand, mediated by the metal d_{z^2} orbital. Transfer of electron density from d_{xy} to d_{z^2} by orbital overlap, however, is forbidden due to the orthogonality of these orbitals. On the other hand, double electron transfer from d_{xy} to d_{z^2} is possible by configuration interaction (CI) and in fact could provide a pathway for N−N cleavage. Nevertheless, the corresponding excited configuration is very high in energy and the interaction with the ground state is weak.[29] Therefore the free activation enthalpy of 31 kcal/mol involved in the N−N cleaving step A represents a lower limit.

Provided the equatorial phosphine ligands remain coordinated, six-coordinate Mo and W hydrazidium complexes thus should be inert to N−N splitting, in agreement with experimental evidence. These systems therefore mark the ultimate stage of N_2 reduction and protonation at d^6 metal centers in the absence of external reductants. To cleave the N−N bond and generate NH_3, electron transfer from an external source is required. However, as the LUMO of the NNH_3 complex is contained in the doubly degenerate set of d_{xz} and d_{yz} metal−N π-antibonding orbitals (cf. Figure 6), reduction of the six-coordinate NNH_3 complexes will eventually lead to splitting of the metal−N bond and loss of the NNH_3 ligand. In practice, two-electron reduction is performed at the NNH_2 stage, primarily leading to elimination of the trans ligand X; subsequent protonation of the resulting five-coordinate, two-electron-reduced NNH_2 species then leads to N−N cleavage and generation of the imido complex.[30] The investigation of this process is the subject of a forthcoming paper.[31]

Acknowledgment. F.T. thanks the State of Schleswig-Holstein for funding of this research and the Fonds der Chemischen Industrie (FCI) for financial support.

Supporting Information Available: Tables of coordinates and matrix values and text discussing correlation energy. This material is available free of charge via the Internet at http://pubs.acs.org.

IC020458X

(28) The temperature in these calculations was set to 298.15 K. $\Delta G°$ was calculated as $\Delta H° - T\Delta S°$.

(29) Cf. Supporting Information.

(30) (a) Hussain, W.; Leigh, G. J.; Pickett, C. J. *J. Chem. Soc, Chem. Commun.* **1982**, 747. (b) Pickett, C. J.; Leigh, G. J. *J. Chem. Soc., Chem. Commun.* **1981**, 1033.

(31) Böres, N.; Horn, K. H.; Lehnert, N.; Mersmann, K.; Tuczek, F. Manuscript in preparation.